PAPER • OPEN ACCESS

Cosmological constraints on curved quintessence

To cite this article: Sukannya Bhattacharya *et al* JCAP09(2024)073

View the article online for updates and enhancements.

Cosmological constraints on curved quintessence

Sukannya Bhattacharya,[a] **Giulia Borghetto,**[b] **Ameek Malhotra,**[b] **Susha Parameswaran,**[c] **Gianmassimo Tasinato**[b,d] **and Ivonne Zavala** [b]

[a]*Dipartimento di Fisica e Astronomia "G. Galilei", Università degli Studi di Padova,*
Via Marzolo 8, 35131 Padova, Italy

[b]*Physics Department, Swansea University,*
Singleton Park, Swansea, SA2 8PP, U.K.

[c]*Department of Mathematical Sciences, University of Liverpool,*
Liverpool, L69 7ZL, U.K.

[d]*Dipartimento di Fisica e Astronomia, Università di Bologna and*
INFN, Sezione di Bologna, I.S. FLAG,
viale B. Pichat 6/2, 40127 Bologna, Italy

E-mail: sukannya.bh@gmail.com, giulia.borghetto@gmail.com,
ameek.malhotra@swansea.ac.uk, susha.parameswaran@liverpool.ac.uk,
g.tasinato2208@gmail.com, e.i.zavalacarrasco@swansea.ac.uk

ABSTRACT: Dynamical dark energy has gained renewed interest due to recent theoretical and observational developments. In the present paper, we focus on a string-motivated dark energy set-up, and perform a detailed cosmological analysis of exponential quintessence with potential $V = V_0 e^{-\lambda\phi}$, allowing for non-zero spatial curvature. We first gain some physical intuition into the full evolution of such a scenario by analysing the corresponding dynamical system. Then, we test the model using a combination of *Planck* CMB data, DESI BAO data, as well as recent supernovae datasets. For the model parameter λ, we obtain a preference for nonzero values: $\lambda = 0.48^{+0.28}_{-0.21}$, $0.68^{+0.31}_{-0.20}$, $0.77^{+0.18}_{-0.15}$ at 68% C.L. when combining CMB+DESI with Pantheon+, Union3 and DES-Y5 supernovae datasets respectively. We find no significant hint for spatial curvature. We discuss the implications of current cosmological results for the exponential quintessence model, and more generally for dark energy in string theory.

Contents

1 Introduction

The ΛCDM model of cosmology has emerged in the last 20+ years as a successful phenomenological model to describe the evolution of our universe from the time of the primordial Big-Bang to today. In this scenario, the present accelerated expansion, discovered at the turn of the 21st century [1, 2], is described by a positive cosmological constant, Λ, while the three-dimensional space curvature is taken to be flat. In recent years, thanks to the explosive increase in the volume and accuracy of cosmological measurements, challenges to this model have started to emerge (see [3] for a recent summary of the so-called cosmological tensions). This is rather good news, as it places us in a remarkable era where fundamental models can be tested and a more accurate cosmological model can emerge. In this work, we study string-motivated dark energy models and confront them with the most recent cosmological data.

Indeed, from the theoretical point of view, much work has been focused on a better understanding of the present (and early) acceleration of the universe and the nature of its source, dark energy, modelled by a cosmological constant in the ΛCDM. Since soon after its discovery, cosmic acceleration has caused concerns due to the appearance of cosmological horizons in eternal acceleration and questions around the consistency of such horizons in a theory of quantum gravity, specifically in string theory [4, 5]. The possibility of realising a de Sitter (dS) universe, namely a universe dominated by a positive cosmological constant, within string theory has subsequently been a source of extensive work and debate (see e.g. [6] for a review). In particular, it has recently been provocatively suggested that dS space cannot arise in string theory and more generally, in quantum gravity [7, 8].

The possibility of a dynamical form of energy, rather than a constant, was put forward early on after the discovery of the late time acceleration, and has received continuous attention thereafter. The main such candidate is *quintessence*, a scalar field whose potential energy drives the accelerated expansion [9–11]. In particular, quintessence models governed by

exponential potentials [12–15], $V = V_0\, e^{-\lambda\phi}$, are especially interesting as they are ubiquitous at the boundaries of moduli spaces in string theory, which are regions that are parametrically under good theoretical control. Cosmological constraints on exponential quintessence with flat spatial slices have been studied recently in [16–18], where upper bounds on the exponent λ were obtained using a combination of *Planck* CMB data, BAO data and supernovae data available at that time. Moreover, in the recent study [18], cosmological constraints of other quintessence potentials were also analysed under the assumption of flat spatial geometry.

Meanwhile, it has been highlighted recently [19] (see also [20]) that including spatial curvature in the context of exponential quintessence may allow for eternally accelerating solutions *without cosmological horizons* for exponents that are well motivated by string theory constructions, $\lambda > \sqrt{2}$. It has also been argued that an open universe is a natural outcome of Coleman-de Luccia tunnelling in the string landscape [21], although other possibilities may also exist, as recently investigated in e.g. [22, 23]. As a further motivation to consider spatial curvature, a recent study [24] (see also [25]) in the context of *islands in cosmology*[1] [28] to understand holography beyond adS/CFT, has found that a small amount of spatial curvature can have a significant effect in the appearance of islands. In particular, in the presence of negative, positive or zero cosmological constant, arbitrarily small positive curvature allows the entire spacetime to be an island. On the other hand, a small amount of negative curvature eliminates cosmological islands entirely.

The full dynamical system including radiation, matter, quintessence and negative spatial curvature was studied in detail not long ago in [29] (see [30] for a review of dynamical systems in cosmology and e.g. [19, 31–34] for some studies of relevant subsystems). An upper bound, $\lambda \lesssim \sqrt{3}$, was found from the minimal phenomenological requirements of a past epoch of radiation domination and acceleration today. Cosmological solutions were shown to start universally in the past from the unique fully unstable fixed-point, a kination epoch, then pass through radiation and matter dominated phases and an epoch of acceleration as finally the unique stable fixed-point is approached. The characteristics of the attractor fixed-point depend on λ; for $\lambda > \sqrt{2}$ it corresponds to a curvature scaling solution, with equation of state $w = -\frac{1}{3}$ whilst for $\lambda \le \sqrt{2}$ it corresponds to scalar domination with $w < -1/3$. How the attractor is approached depends on the initial conditions and consequent trajectory; it turns out that for $\lambda > \sqrt{2}$ and past radiation and matter domination the epoch of acceleration is only transient, whereas for $\lambda \le \sqrt{2}$ the acceleration is eternal and there is an associated cosmological horizon.

Alongside these theoretical developments and motivations, from the cosmological point of view, determining the equation of state of dark energy has been one of the main research motivations and aims of several observational missions such as DES [35], DESI [36], Euclid [37] and LSST [38]. Indeed, recent data from the DES [35] and DESI [36, 39–42] surveys hint at a preference for a dynamical dark energy.[2]

---

[1]Islands have been proposed in the context of the black hole information paradox as hypothetical regions inside the black hole that help encode information from it, ensuring it is not lost in evaporation (see [26] for a review). The boundary of such island is called quantum extremal surface (QES) [27].

[2]See [43–54] for recent discussions related to the interpretations of the DESI results. Refs. [55–58] have also analysed the viability of quintessence models in light of the DESI findings.

These surveys use the so called $w_0 w_a$ or Chevallier-Polarski-Linder (CPL) parameterisation [59, 60] of the equation of state w (at least for small redshifts), which varies linearly with the scale factor a, that is

$$w(a) = w_0 + w_a(1 - a) \,. \tag{1.1}$$

The exponential quintessence model in the presence of spatial curvature has not yet been tested against the most recent cosmological data (see [61] for an early study using WMAP), in particular the late time probes such as BAO from DESI [40], and supernovae datasets such as DES [35], Pantheon+ [62] and Union3 [63].

Therefore, we perform a cosmological analysis of exponential quintessence models in curved space ($k = \pm 1$) using the latest cosmological data (see also appendix B for the flat case $k = 0$). In what follows, we refer to this model as "curved quintessence". When we discuss this model in the context of cosmological constraints, we refer to it as $q\text{CDM}+\Omega_k$ As we will see, including the most recent data from DESI and supernovae data from DES, Pantheon+ and Union3, we are able to constrain the parameter λ, finding it to lie roughly 2–4σ away from $\lambda = 0$ (which represents the cosmological constant), depending on the supernovae dataset chosen. We quantify the improvement in the fit to data provided by the $q\text{CDM}$ model as compared to ΛCDM and also compare this model against the CPL parametrisation, finding a mild preference for the latter.

In section 2 we introduce the cosmological system and perform a dynamical system analysis in 2.1 for the closed case $k = +1$, while the open case $k = -1$ is reproduced from [29] in appendix A (the flat case can be found in [30]). In section 3 we perform the full cosmological analysis of the model with exponential potential for quintessence with curved spacetime geometry. We preset the constraints on the relevant model parameters and discuss their implications. The constraints on the full set of parameters, including 6 base parameters in the standard ΛCDM model, and 2 more for the quintessence model and curvature, are presented in appendix B. Finally in section 4 we summarise our findings.

See [64] for an independent cosmological analysis of curved quintessence and [65] for the analysis in the flat case.

2 Cosmological system

We start by introducing the cosmological system we are interested in analysing: quintessence [9–11] as a possible description of dark energy (DE), together with matter and radiation in a curved space. This constitutes a modification of the standard ΛCDM model, where the cosmological constant Λ, is replaced by a (canonically normalised) scalar field ϕ, and we allow for curvature ($k \neq 0$) of the 3D space slices. The corresponding dynamical analysis is rich in possibilities, which we analyze in this section. In the next sections we study how current data are able to discriminate among different options.

We consider a 4D Friedmann Lemaître Robertson Walker (FLRW) metric with arbitrary curvature given by:

$$ds^2 = -dt^2 + a^2(t) \left[\frac{dr^2}{1 - kr^2} + r^2 \left(d\theta^2 + \sin^2\theta d\psi^2 \right) \right] \,, \tag{2.1}$$

where $k = 0, \pm 1$ denotes the curvature of the three-dimensional (3D) slices. The radiation (r), matter (m) and quintessence field are each described by perfect fluids with energy density, ρ_i, and pressure, p_i, related by their *equation of state* parameter, w_i as:

$$p_i = w_i \rho_i \,, \tag{2.2}$$

with $i = r, m, \phi$, respectively. For radiation, $\rho_r \sim a^{-4}$ and $w_r = \frac{1}{3}$; for matter, $\rho_m \sim a^{-3}$ and $w_m = 0$; for the scalar, the energy density and pressure are given by

$$\rho_\phi = \frac{\dot{\phi}^2}{2} + V(\phi) \,, \qquad p_\phi = \frac{\dot{\phi}^2}{2} - V(\phi) \,. \tag{2.3}$$

Moreover, we can introduce an effective "curvature fluid component", with energy density, pressure and equation of state given by

$$\rho_k = -\frac{3\,k}{a^2} \,, \qquad p_k = \frac{k}{a^2} \,, \qquad w_k = -\frac{1}{3} \,. \tag{2.4}$$

The equations of motion for this system are given by (we set $M_{\mathrm{Pl}}^{-2} = 8\pi G = 1$ in this section):

$$H^2 = \frac{\rho_{\mathrm{eff}}}{3} \,, \tag{2.5a}$$

$$-\frac{\dot{H}}{H^2} = \frac{3}{2}(1 + w_{\mathrm{eff}}) \,, \tag{2.5b}$$

$$\ddot{\phi} = -3H\dot{\phi} - V_\phi \,. \tag{2.5c}$$

In these equations, $V_\phi \equiv \partial_\phi V$ and we defined

$$\rho_{\mathrm{eff}} = \sum_n \rho_n \,, \qquad p_{\mathrm{eff}} = \sum_n p_n \,, \qquad p_{\mathrm{eff}} = w_{\mathrm{eff}}\, \rho_{\mathrm{eff}}, \tag{2.6}$$

with $n = r, m, \phi, k$, that is, running over radiation, matter, the scalar and curvature terms. From this definition we can deduce that

$$w_{\mathrm{eff}} = \sum_n w_n \Omega_n \,. \tag{2.7}$$

Moreover, from (2.5b), one can check that cosmic acceleration requires

$$w_{\mathrm{eff}} < -1/3 \quad \Leftrightarrow \quad \epsilon \equiv -\dot{H}/H^2 < 1 \,. \tag{2.8}$$

Introducing the density parameters for each component, n, in the universe as

$$\Omega_n = \frac{\rho_n}{3H^2} \,, \tag{2.9}$$

we can write the first Friedmann equation as

$$1 = \sum_n \Omega_n \,, \qquad \text{or} \qquad 1 - \Omega_k = \Omega_T, \tag{2.10}$$

where

$$\Omega_T = \sum_i \Omega_i \,. \tag{2.11}$$

From (2.10), we see the standard result that in an open universe $(k = -1)$, $\Omega_T < 1$, in a closed universe $(k = 1)$, $\Omega_T > 1$ and in a flat universe $\Omega_T = 1$.

For the rest of our analysis we restrict ourselves to an exponential potential for the scalar field, given by

$$V(\phi) = V_0 \, e^{-\lambda\phi} \,, \tag{2.12}$$

where λ is a constant and we take $\lambda > 0$, $V_0 \geq 0$. As discussed in the Introduction, this is motivated from the general form of a perturbatively generated potential for a closed string modulus after canonical normalisation (see e.g. [6]).

2.1 Dynamical systems analysis

To study the background evolution of the system, it is useful to translate the equations of motion into an autonomous system of first order coupled differential equations, and perform a dynamical systems analysis. Curved exponential quintessence including a barotropic fluid has been studied previously in [31] and in [32] an analysis was performed including matter and radiation (see also [30] for a review on dynamical systems in cosmology and references therein). More recently, in [29] the open case ($k = -1$) including radiation and matter was studied in detail. We refer the reader to that paper for details and present a summary of their main results in appendix A. Below we give some details on the closed case ($k = +1$). As pointed out in [30, 31], the dynamical system in the closed case is non-compact.

We define the following dynamical system variables:

$$\bar{x} = \frac{\phi'}{\sqrt{6}} \,, \qquad \bar{y} = \frac{\sqrt{V}}{\sqrt{3}\bar{H}} \,, \qquad \bar{u} = \frac{\sqrt{\rho_r}}{\sqrt{3}\bar{H}} \,, \qquad \bar{z} = \frac{H}{\bar{H}} \,, \qquad \lambda = -\frac{V_\phi}{V} \,, \tag{2.13}$$

together with the constraint

$$\bar{\Omega}_m = 1 - \bar{x}^2 - \bar{y}^2 - \bar{u}^2 \,, \tag{2.14}$$

where

$$\bar{\Omega}_m \equiv \frac{\rho_m}{3\bar{H}^2} \,, \tag{2.15}$$

and, importantly, we introduce

$$\bar{H} = H\sqrt{1 - \Omega_k} \,, \quad \text{where} \quad \Omega_k \equiv -\frac{k}{a^2 H^2} \,, \quad \text{and} \quad k > 0 \,, \tag{2.16}$$

to compactify our phase space [30]. Primes above denote derivatives with respect to the new e-fold variable:

$$d\bar{N} = \bar{H}dt \,. \tag{2.17}$$

The equations of motion (2.5) can be rewritten in terms of variables (2.13) as follows:

$$\bar{x}' = \frac{1}{2}\,\bar{x}\,\bar{z}\left(-3 + \bar{u}^2 + 3\bar{x}^2 - 3\bar{y}^2\right) + \sqrt{\frac{3}{2}}\lambda\,\bar{y}^2 \,, \tag{2.18a}$$

$$\bar{y}' = \frac{1}{2}\,\bar{y}\,\bar{z}\left(3 + \bar{u}^2 + 3\bar{x}^2 - 3\bar{y}^2\right) - \sqrt{\frac{3}{2}}\,\lambda\,\bar{x}\,\bar{y} \,, \tag{2.18b}$$

$$\bar{u}' = \frac{1}{2}\,\bar{u}\,\bar{z}\left(-1 + \bar{u}^2 + 3\bar{x}^2 - 3\bar{y}^2\right) \,, \tag{2.18c}$$

$$\bar{z}' = \frac{1}{2}\left(\bar{z}^2 - 1\right)\left(1 + \bar{u}^2 + 3\bar{x}^2 - 3\bar{y}^2\right) \,, \tag{2.18d}$$

$$\lambda' = -\sqrt{6}\,\bar{x}\left[\frac{V_{\phi\phi}}{V} - \frac{V_\phi^2}{V^2}\right] \,. \tag{2.18e}$$

$(\bar{x}, \bar{y}, \bar{z}, \bar{u})$	$\bar{\Omega}_m$	Existence	w_{eff}
$\bar{Q}_{\text{kin}}^{\pm} = (\pm 1, 0, 1, 0)$	0	$\forall \lambda$	1
$\bar{Q}_m = (0, 0, 1, 0)$	1	$\forall \lambda$	0
$\bar{Q}_{k\phi} = \left(\frac{1}{\sqrt{3}}, \pm\sqrt{\frac{2}{3}}, \frac{\lambda}{\sqrt{2}}, 0\right)$	0	$\lambda < \sqrt{2}$ (For $\lambda = \sqrt{2}$, $\bar{Q}_{k\phi} = \bar{Q}_{\phi}$)	$-\frac{1}{3}$
$\bar{Q}_{\phi} = \left(\frac{\lambda}{\sqrt{6}}, \pm\frac{\sqrt{6-\lambda^2}}{\sqrt{6}}, 1, 0\right)$	0	$\lambda < \sqrt{6}$ (For $\lambda = \sqrt{6}$, $\bar{Q}_{\phi} = \bar{Q}_{\text{kin}}^{+}$)	$\frac{\lambda^2}{3} - 1$
$\bar{Q}_{m\phi} = \left(\frac{1}{\lambda}\sqrt{\frac{3}{2}}, \pm\frac{1}{\lambda}\sqrt{\frac{3}{2}}, 1, 0\right)$	$1 - \frac{3}{\lambda^2}$	$\lambda > \sqrt{3}$ (For $\lambda = \sqrt{3}$, $\bar{Q}_{m\phi} = \bar{Q}_{\phi}$)	0
$\bar{Q}_r = (0, 0, 1, \pm 1)$	0	$\forall \lambda$	$\frac{1}{3}$
$\bar{Q}_{r\phi} = \left(\frac{1}{\lambda}\sqrt{\frac{8}{3}}, \pm\frac{2}{\lambda\sqrt{3}}, 1, \pm\sqrt{1 - \frac{4}{\lambda^2}}\right)$	0	$\lambda > 2$ (For $\lambda = 2$, $\bar{Q}_{r\phi} = \bar{Q}_{\phi}$)	$\frac{1}{3}$

Table 1. Fixed points for the system (2.18) with the constraint (2.14) and the exponential potential (2.12). See the main text for their description.

The fixed points for this system are given in table 2 below; since we are interested only in expanding universes, we stick there to the case $\bar{z} > 0$. The stability of the closed universe fixed points is summarised in table 7. For comparison, the fixed points for the open case as well as their properties and stability as discussed in [29] are reproduced in appendix A.

Let us now discuss the properties and stability of the fixed points in the closed case.

- $\bar{Q}_{\text{kin}}^{\pm}$ — *kinetic domination*: the energy density is dominated by the kinetic energy of the scalar field, with $\bar{x}^2 = 1$, and thus $w_{\text{eff}} = 1$. These points are the only fully unstable fixed points, and thus all cosmological trajectories originate near them in the far past. This is analogous to the open case.

- $\bar{Q}_m$ — *matter domination*: the energy density is dominated by matter, $\bar{\Omega}_m = 1$, and thus $w_{\text{eff}} = 0$. This point is a saddle and thus cosmological trajectories may pass through it depending on the initial conditions. This is analogous to the point P_m in the open case (see table 7).

- $\bar{Q}_{k\phi}$ — *curvature scaling*: at this point the universe evolves under the influence of both curvature and the scalar field, but the expansion mimics curvature domination with $w_{\text{eff}} = -\frac{1}{3}$. This is analogous to the $P_{k\phi}$ point in the open case (see table 7), however, the existence condition is the opposite: $\lambda < \sqrt{2}$. Contrary to the open case, this point is a saddle in the closed case.

- $\bar{Q}_\phi$ — *scalar domination*: the energy density is dominated by the scalar, with $w_{\text{eff}} = w_\phi$ and $\bar{\Omega}_\phi = 1$. This is analogous to the point P_ϕ in the open case and the stability properties are the same: stable for $\lambda \leq \sqrt{2}$, saddle otherwise. For $\lambda < \sqrt{2}$ it therefore represents the late-time accelerating attractor for all cosmological trajectories.

- $\bar{Q}_{m\phi}$ — *matter scaling*: the evolution is driven by the scalar and matter energy densities, but mimics a matter dominated evolution, with $w_{\text{eff}} = 0$ and $\bar{\Omega}_m = 1 - 3/\lambda^2$. This is analogous to the point $P_{m\phi}$ in the open case and it is a saddle.

- $\bar{Q}_r$ — *radiation domination*: The energy density is dominated entirely by radiation with $w_{\text{eff}} = 1/3$. This is analogous to the point P_r in the open case and it is a saddle.

- $\bar{Q}_{r\phi}$ — *radiation scaling*: the evolution is driven by both the scalar and radiation, though the evolution mimics a radiation dominated universe with $w_{\text{eff}} = \frac{1}{3}$, while $\bar{\Omega}_r = \bar{u}^2 = 1 - 4/\lambda^2$. This is a saddle point and it is analogous to the point $P_{r\phi}$ in the open case.

In summary, there are three main differences with the open universe case (see tables 7 and 8 in appendix A). The first is that in the closed case there is no curvature dominated point, as expected (in the open case, this is P_k in table 8). The second is that the curvature scaling point is not stable, and its existence condition is complementary to the open case: $\lambda < \sqrt{2}$ vs. $\lambda > \sqrt{2}$, for the closed and open case respectively. Finally, whilst both the open and closed universe systems have a scalar dominated fixed point attractor when $\lambda < \sqrt{2}$, when $\lambda > \sqrt{2}$ the open universe has a curvature scaling fixed point attractor but the closed universe system has no attractor. In other words, for the closed universe, the entire cosmological trajectory depends on the initial conditions.

In figure 1 we present an example slice of the dynamical systems phase space for $\lambda = \sqrt{8/3}$, choosing to present the variables $\bar{x}, \bar{y}$ and $\sqrt{\bar{\Omega}_m}$ and dropping $\bar{u}$ and $\bar{z}$ (but recall the constraint $\bar{\Omega}_m = 1 - \bar{x}^2 - \bar{y}^2 - \bar{u}^2$). We also plot in the phase space an example trajectory, with initial conditions fixed by present-day values for the density parameters and w_ϕ, chosen to match the CAMB runs described in the following subsection. We learn that the cosmological solution starts in a kination epoch, from the fixed point $\bar{Q}_{\text{kin}}^+$, passes through radiation and matter domination as it approaches $\bar{Q}_m$ and $\bar{Q}_r$, respectively, meets the point corresponding to today (as it must), where there is transient acceleration, and eventually returns to $\bar{Q}_{\text{kin}}^+$, another kination epoch. Recall that the latter fixed point is a saddle, thus we do not expect it to be a final destination. See [29] for similar phase space diagrams for the open universe.

2.2 Background evolution

We now study the cosmological evolution of the curved exponential quintessence. We implement the curved quintessence model in the cosmological Boltzmann code CAMB [66, 67]. We choose initial conditions for the field: $\phi_i = 0$, $\dot{\phi}_i = 0$, deep in the radiation era.[3] For a given input value of λ and other background density parameters $\{\Omega_{\text{b}}, \Omega_{\text{c}}, \Omega_k, \Omega_{\text{r}}\}$, the

---

[3]Note that a non-zero value of ϕ_i can be absorbed into a redefinition of V_0. Moreover, any non-zero initial velocity is quickly washed out due to Hubble friction.
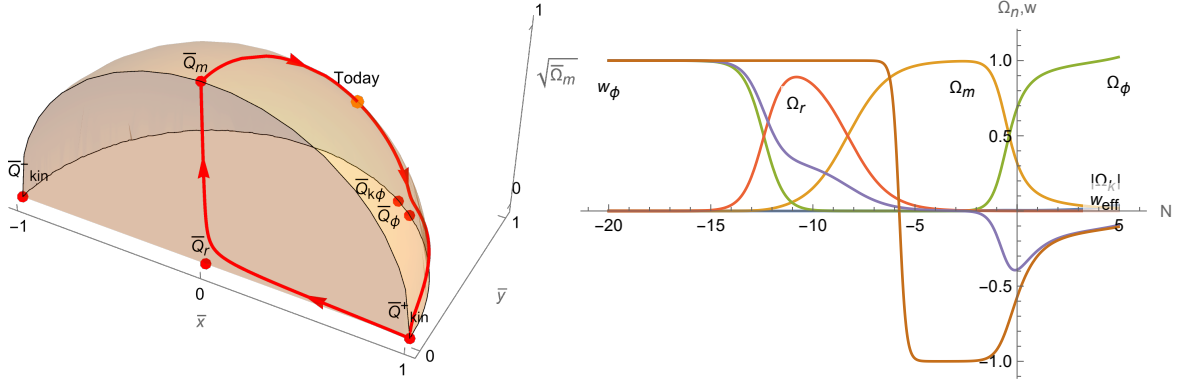
Figure 1. *Left:* a slice of the phase space for the dynamical system including quintessence, matter, radiation and positive spatial curvature, with the selection of variables $\bar{x}$, $\bar{y}$ and $\sqrt{\bar{\Omega}_m}$, for $\lambda = \sqrt{8/3}$. Plotted in red is the trajectory determined by the initial conditions set today by $\Omega_{k,0} = -0.005000423845$, $\Omega_{\phi,0} = 0.684587702938$, $\Omega_{r,0} = 0.000080007654$ and $w_{\phi,0} = -0.573508930813358$, with: $\bar{z}_0 = 1/\sqrt{1-\Omega_{k,0}}$, $\bar{x}_0 = \sqrt{\Omega_{\phi,0}\bar{z}_0^2(1+w_{\phi,0})/2}$, $\bar{y}_0 = \sqrt{\Omega_{\phi,0}\bar{z}_0^2 - \bar{x}_0^2}$, $\bar{u}_0 = \sqrt{\Omega_{r,0}}\bar{z}_0$. These values are taken from the run of CAMB described in the following section, with a large amount of precision necessary to ensure past radiation domination. *Right:* The corresponding evolution of density parameters, Ω_n (Ω_ϕ in green, Ω_r in red, Ω_m in yellow, and Ω_k in blue) and equations of state (w_ϕ in brown and $w_{\rm eff}$ in purple), with respect to N, related to $\bar{N}$ as $dN = \bar{z}d\bar{N}$. See main text for more details.

Point	Eigenvalues	Stability	Existence
$\bar{Q}_{\rm kin}^\pm$	$\left(4, 3, 3 \mp \lambda\sqrt{\frac{3}{2}}, 1\right)$	$\bar{Q}_{\rm kin}^-$: Fully unstable $\bar{Q}_{\rm kin}^+$: Fully unstable for $\lambda \leq \sqrt{6}$ $\bar{Q}_{\rm kin}^+$: Saddle for $\lambda > \sqrt{6}$	—
$\bar{Q}_k$	$(-\frac{3}{2}, \frac{3}{2}, -\frac{1}{2}, 1)$	Saddle	—
$\bar{Q}_{k\phi}$	$\left(-\frac{\lambda}{\sqrt{2}}, -\frac{\lambda}{\sqrt{2}}, \frac{-\lambda+\sqrt{8-3\lambda^2}}{\sqrt{2}}, -\frac{\lambda+\sqrt{8-3\lambda^2}}{\sqrt{2}}\right)$	Saddle	$\lambda < \sqrt{2}$
$\bar{Q}_\phi$	$\left(\frac{\lambda^2}{2} - 3, \frac{\lambda^2}{2} - 3, \lambda^2 - 2, \lambda^2 - 2\right)$	Stable for $\lambda < \sqrt{2}$ Saddle for $\lambda > \sqrt{2}$	$\lambda < \sqrt{6}$
$\bar{Q}_{m\phi}$	$\left(-\frac{1}{2}, 1, \frac{3(-\lambda+\sqrt{24-7\lambda^2})}{4\lambda}, -\frac{3(\lambda+\sqrt{24-7\lambda^2})}{4\lambda}, -\frac{1}{2}\right)$	Saddle	$\lambda > \sqrt{3}$
$\bar{Q}_r$	$(2, 2, 1, -1)$	Saddle	—
$\bar{Q}_{r\phi}$	$\left(1, 2, \frac{-\lambda+\sqrt{64-15\lambda^2}}{2\lambda}, -\frac{\lambda+\sqrt{64-15\lambda^2}}{2\lambda}\right)$	Saddle	$\lambda > 2$

Table 2. Summary of the stability analysis for the fixed points in table 2 corresponding to a closed universe.

λ	V_0 (eV^2)	$w_{\phi,0}$
0.5	1.0715×10^{-7}	-0.96369
$\sqrt{8/3}$	2.1765×10^{-7}	-0.58169
$\sqrt{3}$	2.5255×10^{-7}	-0.52205
2	4.8067×10^{-7}	-0.32093

Table 3. Parameter values for $k < 0$ for the plots in figures 2, 3 and 4 as computed from CAMB. The associated values for today's density parameters are $\Omega_{k,0} = 0.00500$, $\Omega_{c,0} = 0.27018$, $\Omega_{b,0} = 0.04872$, and $\Omega_{\phi,0} = 0.67459$.

amplitude of the potential V_0 is tuned by the code and adjusted to obtain the correct Ω_ϕ today, in order to satisfy eq. (2.10).

We consider two cases motivated by string theory set-ups as discussed in [29], $\lambda = \sqrt{3}, \sqrt{8/3}$, as well as a larger and smaller value motivated by our further cosmological analysis in the next section. The field typically remains frozen due to Hubble friction in the radiation era and starts to evolve much later when dark energy begins to dominate (see figures 4, 7 below). We can understand the evolution from the dynamical system analysis. For $\lambda = \sqrt{3}$, for both open and closed universes, the matter scaling points merge with the scalar dominated point: $P_{m\phi} = P_\phi$ and $\bar{Q}_{m\phi} = \bar{Q}_\phi$ respectively. For the open case, there is a curvature scaling point $P_{k\phi}$, but not in the closed case. For $\lambda = \sqrt{8/3}$, for both closed and open universes, the matter scaling points do not exist, while the scalar dominated points still exist and are saddles ($P_\phi, \bar{Q}_\phi$). Further, the open curvature scaling point ($P_{k\phi}$) also exists (and is stable). Finally we also plot the evolution for $\lambda = 1/2$ and $\lambda = 2$. For $\lambda = 1/2$ the closed curvature scaling point exists, but not for the open case. The scalar dominated point instead exists for both open and closed cases, it gives rise to acceleration and it is stable. For $\lambda = 2$, the closed scaling point does not exist, but it does for the open case, while the scalar dominated point exists in both cases and it is a saddle. For all the values of $\lambda < \sqrt{2}$, the scalar fixed point is an accelerating attractor. In this case, the universe will evolve towards an accelerating future with a cosmological horizon.

2.2.1 Open universe

In figure 2 we show the evolution of the curvature and scalar density parameters for the values of λ described therein (at the top left panel). In the bottom left panel, we show the deviation of our model from ΛCDM by plotting the temperature angular power spectrum $D_\ell^{TT} \equiv \ell(\ell+1)C_\ell^{TT}/(2\pi)$, and we plot the difference $\Delta D_\ell^{TT} \equiv D_\ell^{TT,\Lambda\text{CDM}} - D_\ell^{TT,q\text{CDM}+\Omega_k}$ in the bottom right panel.

In figure 3 we show the evolution of the corresponding scalar and effective equations of state, w_ϕ and w_{eff}. The values of the parameters today together with V_0, as computed by CAMB, are given in table 3.

2.2.2 Closed universe

In figure 5 we show the evolution of the density parameters as well as the angular power spectrum D_ℓ^{TT} and ΔD_ℓ^{TT}, for the values of λ described above. In figure 6 we show evolution
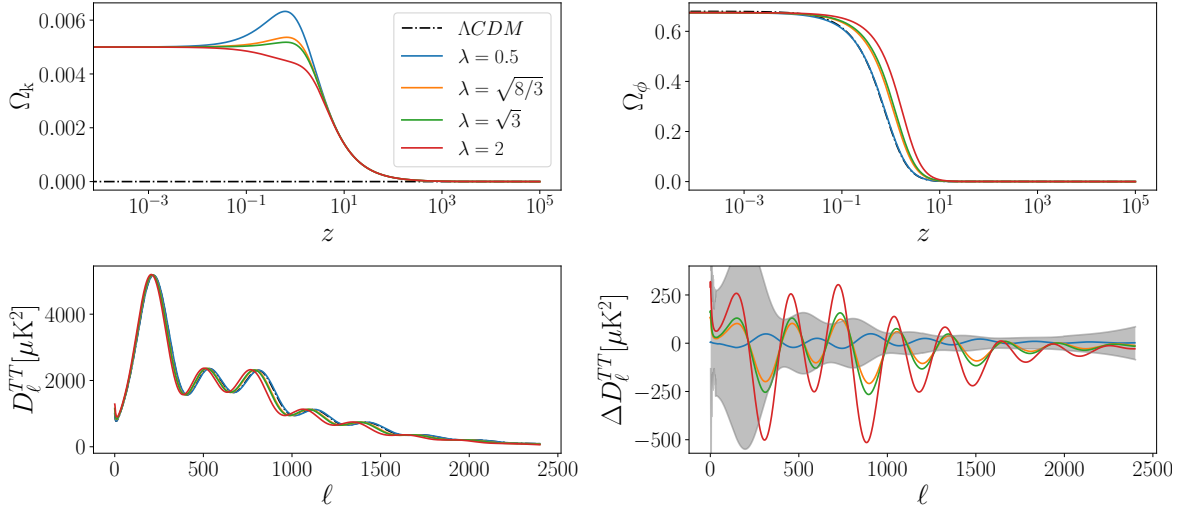
Figure 2. *Upper panel*: Curvature and scalar density parameter evolution for various values of λ for an open universe $k < 0$. *Lower panel*: angular power spectrum D_ℓ^{TT} and the residuals ΔD_ℓ^{TT} with respect to ΛCDM, for the same values of λ and $k < 0$. The grey shaded regions represent the error bars on D_ℓ^{TT} from *Planck* [68].
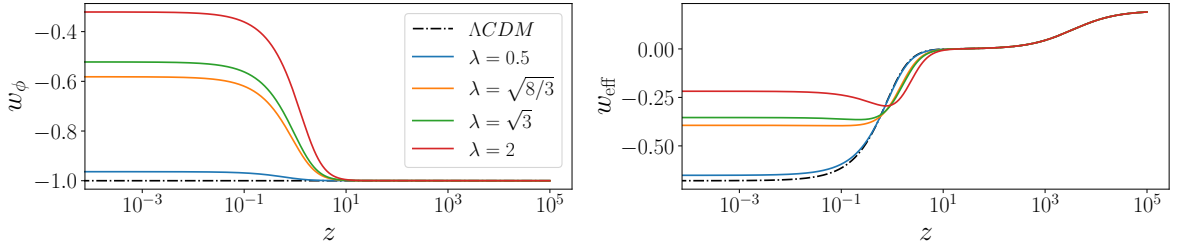
Figure 3. Equations of state evolution for the same parameter values as in figure 2 computed from CAMB.
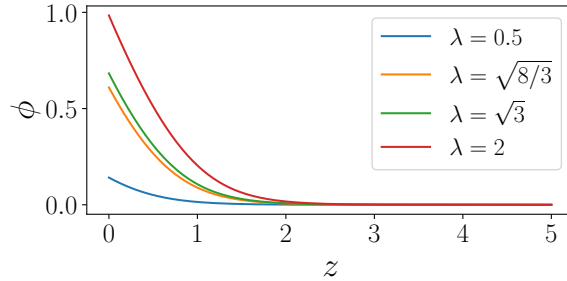

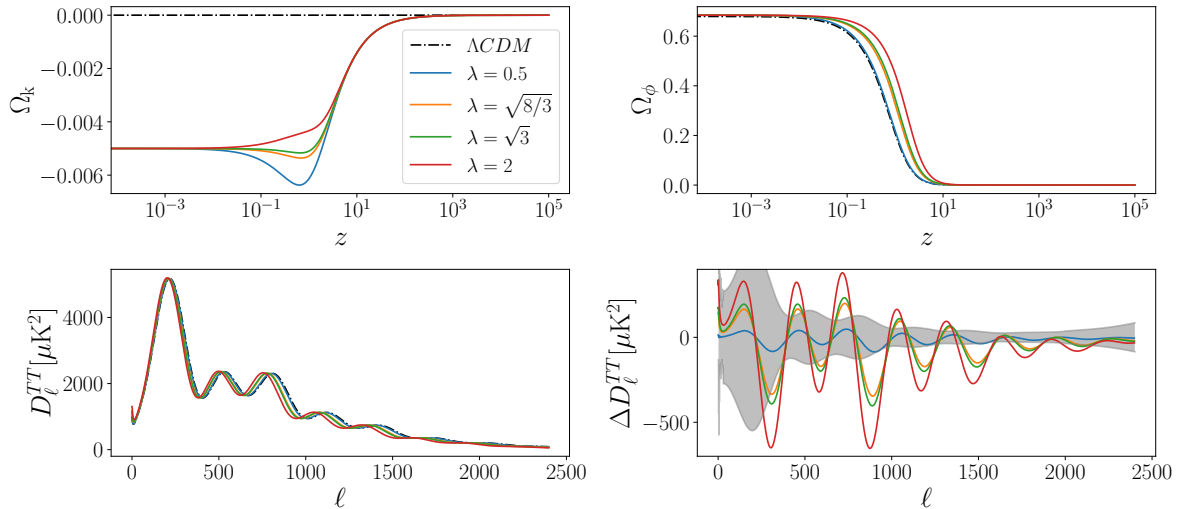**Figure 4.** Scalar field evolution for the open quintessence case.

Figure 5. Curvature and scalar density parameter evolution for a closed universe, $k > 0$ for various values of λ (upper panel). Angular power spectrum D_ℓ^{TT} and residuals ΔD_ℓ^{TT} for same values of λ and $k > 0$ (lower panel). The grey shaded regions represent the error bars on D_ℓ^{TT} from *Planck* [68].
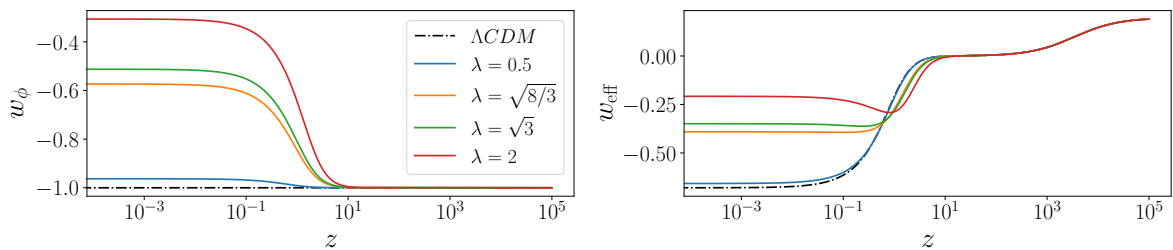

Figure 6. Evolution of the equations of state for $k > 0$ for the different values of λ discussed in the text.
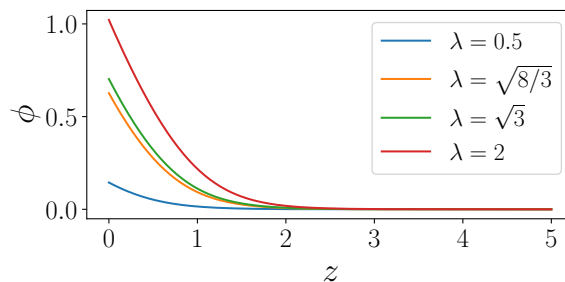

Figure 7. Scalar field evolution for the closed quintessence case.

of the scalar and effective equations of state and in figure 7 we show the corresponding evolution of the scalar field. The values of current-day parameters as computed from `CAMB` for these cases are given in table 4.

Comparing the open and closed universes, we learn that the closed universe yields slightly higher values for the dark energy density parameter today, Ω_ϕ^0, for a given λ. This is to be expected from (2.10). On the other hand, the value of w_ϕ for a given λ is slightly less negative in the closed case (see table 3 and table 4).

λ	V_0 (eV^2)	$w_{\phi,0}$
0.5	1.0886×10^{-7}	-0.96300
$\sqrt{8/3}$	2.2576×10^{-7}	-0.57350
$\sqrt{3}$	2.6350×10^{-7}	-0.51259
2	5.1973×10^{-7}	-0.30628

Table 4. Parameter values as computed from `CAMB` for the plots in figures 5, 6 and 7 ($k > 0$). The associated values for today's density parameters are $\Omega_{k,0} = -0.00500$, $\Omega_{c,0} = 0.27018$, $\Omega_{b,0} = 0.04872$, and $\Omega_{\phi,0} = 0.68459$.

3 Cosmological constraints

With the modified `CAMB` code, we are now ready to analyse our curved quintessence model against cosmological datasets. We explore the parameter space of the model using Markov Chain Monte-Carlo (MCMC) methods, varying λ alongside the other cosmological parameters $\{\Omega_b h^2, \Omega_c h^2, \Omega_k, H_0, \tau, A_s, n_s\}$.[4] We use the following cosmological likelihoods:

1. CMB from *Planck*:

   - *Planck* 2018 low-ℓ temperature and polarisation likelihood [68].
   - *Planck* high-ℓ CamSpec TTTEEE temperature and polarization likelihood using `NPIPE` (*Planck* PR4) data [69].
   - *Planck* 2018 lensing likelihood [70].

   In what follows, we collectively denote all the *Planck* likelihoods as 'CMB'.[5]

2. BAO likelihoods from DESI DR1 [36, 39, 40] consisting of bright galaxy survey (BGS), luminous red galaxies (LRG), emission line galaxies (ELG), quasars and Lyman-α (Lyα) data which cover a total redshift range $0.1 < z < 4.2$. Sloan Digital Sky Survey (SDSS) DR16 likelihoods [71] covering a total redshift range $0.07 < z < 3.5$ for the ELG, LRG, quasar and Lyα tracers.

3. Pantheon+ [62], Union3 [63] and DES-Y5 [35] type Ia supernovae samples. Altogether, these samples consist of about 4000 supernovae which cover a redshift range $0.001 < z < 2.26$. Note that the samples cannot be combined since Pantheon+ and Union3 have 1363 supernovae in common while DESY5 has 194 low redshift supernovae shared with the other two.

---

[4]The parameter λ is the only free parameter of the quintessence model since V_0 is getting tuned at each step of the MCMC to satisfy the budget equation (2.10).

[5]Note that the *Planck* high-ℓ and lensing likelihoods require the modelling of non-linear scales by codes such as HMcode/halofit, which do not have a quintessence background evolution. Thus, the effects of quintessence on these non-linear scales cannot be accounted for here. However, we expect the corrections from non-linear scales on our conclusions about evolving dark energy to be quite small at present. In particular, the preference for dynamical dark energy is primarily driven by the BAO and SN datasets for which the observables are mainly background quantities and thus should not be affected by non-linear physics.
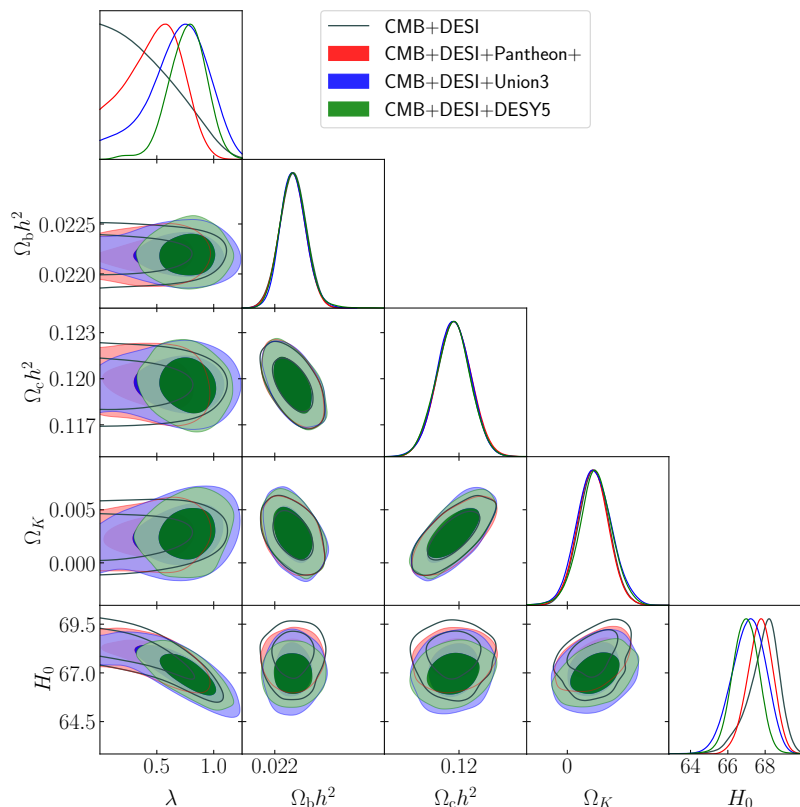
Figure 8. Constraints on cosmological parameters from the combinations of datasets described in the main text. See appendix B for the inclusion of all the other parameters.

We implement wide uniform priors on all the cosmological parameters. The likelihoods are sampled using the `MCMC` sampler [72, 73], through its interface with `Cobaya` [74]. We continue the sampling until we reach a value $R - 1 = 0.03$ for the Gelman-Rubin diagnostic. The resulting chains are analysed and plotted with `GetDist` package [75]. At the end of the sampling, we also run the `Py-BOBYQA` [76, 77] minimizer through the `Cobaya` interface to find the best-fit point and the corresponding χ^2 values.

The recent DESI BAO data alone, as well as in conjunction with the supernovae datasets, have already been shown to have a preference for a time varying dark energy equation of state as compared to ΛCDM [40–42]. When the same datasets are used with our exponential quintessence model as the underlying dark energy model, this manifests as a slight preference for a non-zero λ, resulting in the following marginalised mean and limits (at 68% C.L) shown in table 5.[6]

The marginalised 1D and 2D joint distributions for these parameters are plotted in figure 8. As we can see, the combination of CMB and DESI BAO data is not able to significantly constrain the quintessence model parameter λ. However, this changes with the addition of the supernovae datasets and depending on the dataset chosen, the obtained values for λ lie about 2–4σ away from the $\lambda = 0$ case that corresponds to a cosmological constant. In appendix B,

---

[6]The datasets we use correspond to slightly different values of H_0 (see table 9), decreasing with increasing values of λ, a trend consistent with previous works [78, 79] for the flat case.

Parameter	CMB+DESI	+Pantheon+	+Union3+	+DESY5
λ	< 0.537	$0.48^{+0.28}_{-0.21}$	$0.68^{+0.31}_{-0.20}$	$0.77^{+0.18}_{-0.15}$
Ω_k	0.0026 ± 0.0015	0.0025 ± 0.0015	$0.0028^{+0.0016}_{-0.0019}$	0.0027 ± 0.0016
$\Omega_c h^2$	0.1196 ± 0.0012	0.1197 ± 0.0012	0.1195 ± 0.0012	0.1195 ± 0.0012
H_0	$67.89^{+0.96}_{-0.61}$	$67.73^{+0.72}_{-0.64}$	$67.12^{+0.97}_{-0.83}$	66.95 ± 0.72
$\Omega_b h^2$	0.02219 ± 0.00014	0.02219 ± 0.00013	$0.02220^{+0.00013}_{-0.00015}$	0.02221 ± 0.00013

Table 5. Parameter means and 68% limits for the combination of the CMB+DESI and with the addition of the different supernovae datasets to the CMB+DESI baseline.

Parameter	CMB+DESI+Pantheon+	CMB+SDSS+Pantheon+
λ	$0.48^{+0.28}_{-0.21}$	$0.40^{+0.20}_{-0.29}$
Ω_k	0.0025 ± 0.0015	0.0014 ± 0.0017
$\Omega_c h^2$	0.1197 ± 0.0012	$0.1197^{+0.0013}_{-0.0012}$
H_0	$67.73^{+0.72}_{-0.64}$	67.44 ± 0.64
$\Omega_b h^2$	0.02219 ± 0.00013	$0.02220^{+0.00013}_{-0.00016}$

Table 6. Parameter means and 68% limits.

we plot the contours for the full parameter set, including $\{n_s, A_s, \tau\}$. There, we also present the results of the MCMC analysis for the dataset combination CMB+DESI+Pantheon+, fixing $\Omega_k = 0$ and compare it to the free spatial curvature case (figure 13). We do not find any major difference for the cosmological parameters constraints, in particular for λ, obtaining $\lambda = 0.42 \pm 0.22$ at 68% C.L.

Fixing our supernovae dataset to Pantheon+, we also assess the effect of replacing the full DESI BAO data with the SDSS data, finding nearly identical results for most cosmological parameters with a slightly lower deviation from a cosmological constant in terms of the preferred values of λ (see figure 9 and table 6). The result could be attributed to the increased constraining power of the DESI data as compared to SDSS. For all the datasets used in this section, we also observe a mild shift towards $\Omega_k > 0$ with the difference from $\Omega_k = 0$ being less than 2σ. There is no noticeable shift for any of the other cosmological parameters.

Considering that the new DESI dataset favours dynamical dark energy, we can compare how well our model fits the data against the CPL parametrisation presented in [40]. For this, we first compute the $\Delta\chi^2$ for both the qCDM+Ω_k model and the $w_0 w_a$CDM+Ω_k model with respect to ΛCDM $+\Omega_k$, i.e.

$$\Delta\chi^2_{\text{model}} \equiv \chi^2_{\text{model}} - \chi^2_{\Lambda\text{CDM}+\Omega_k}, \tag{3.1}$$

where the $\chi^2 = -2\ln\mathcal{L}_{\text{max}}$ for a given model. We find for the CMB+DESI+Pantheon+ combination

$$\Delta\chi^2_{q\text{CDM}+\Omega_k} = -1.8 \qquad \text{and} \qquad \Delta\chi^2_{w_0 w_a\text{CDM}+\Omega_k} = -6, \tag{3.2}$$
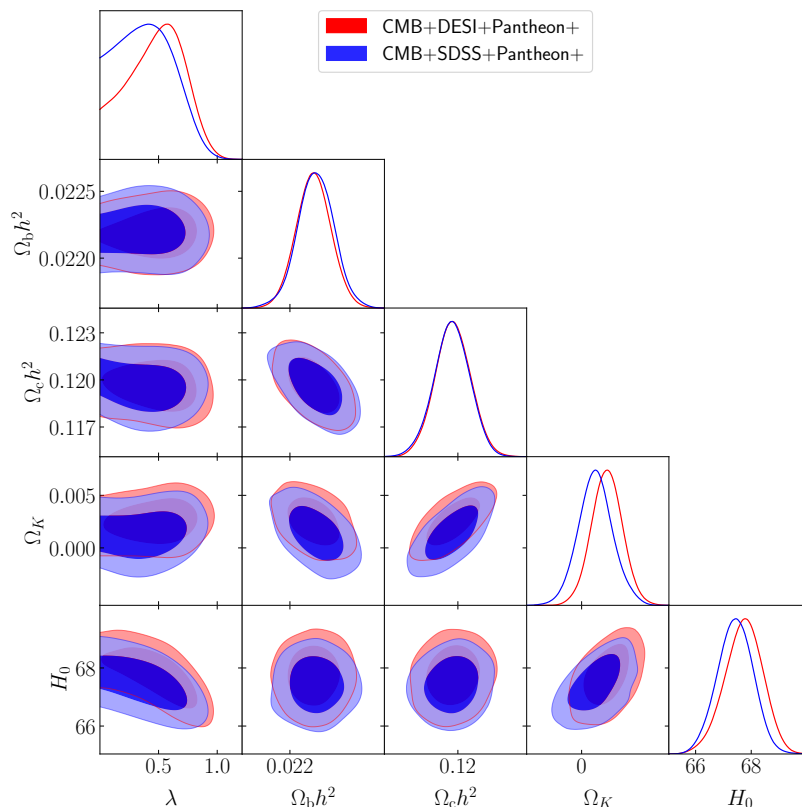
Figure 9. Constraints on cosmological parameters for CMB+DESI+Pantheon+ and CMB+SDSS+Pantheon+. See appendix B for the inclusion of all the other parameters.

showing that both models provide a better fit to the data compared to ΛCDM+Ω_k. This is to be expected since we can always recover ΛCDM+Ω_k from the two models by fixing, respectively, $\lambda = 0$ or $w_0 = -1$, $w_a = 0$. We remind the reader that the qCDM+Ω_k model features one additional parameter compared to ΛCDM+Ω_k whereas the $w_0 w_a$ model has two.

When comparing cosmological models using their best-fit χ^2 values, one should also take into account the number of free parameters of the model. For non-nested models,[7] a simple method to compare the quality of the fit to the data while at the same time accounting for the number of model parameters is provided by the Akaike information criterion (AIC) [80, 81]. We compute this quantity for the qCDM+Ω_k and $w_0 w_a$CDM+Ω_k models. The AIC value for a given model is defined as

$$\text{AIC} = 2n - 2\ln\mathcal{L}_{\max}, \tag{3.3}$$

where $\mathcal{L}_{\max}$ denotes the maximum likelihood value for the model and n is the number of free parameters (note $n_{w_0 w_a \text{CDM}} - n_{q\text{CDM}} = (7+2) - (7+1) = 1$). AIC represents the information loss in using a particular model to represent the true underlying process with the best fitting model among the candidate models having the smallest AIC value, i.e. the lowest information

---

[7]It is only for nested models that the maximum (log) likelihood ratio or $\Delta\chi^2$ is approximately χ^2 distributed [80]. The AIC has no such requirement but is a simplistic comparison method. A more rigorous comparison would be to compute the Bayesian evidences but this is computationally quite expensive.

loss [80, 81]. For our analysis with CMB+DESI+Pantheon+, we find

$$\text{AIC}_{w_0 w_a \text{CDM}+\Omega_k} - \text{AIC}_{q\text{CDM}+\Omega_k} = -2.2, \quad \text{AIC}_{q\text{CDM}+\Omega_k} - \text{AIC}_{\Lambda\text{CDM}+\Omega_k} = 0.2 \qquad (3.4)$$

which indicates a preference, albeit not very strong, for the $w_0 w_a$ parametrisation over the exponential quintessence model and no preference between $q\text{CDM}+\Omega_k$ and $\Lambda\text{CDM}+\Omega_k$. On replacing the Pantheon+ dataset with Union3 or DESY5, the results change slightly. For example, for CMB+DESI+Union3, we find:[8]

$$\text{AIC}_{w_0 w_a \text{CDM}+\Omega_k} - \text{AIC}_{q\text{CDM}+\Omega_k} = -3 \quad \text{and} \quad \text{AIC}_{q\text{CDM}+\Omega_k} - \text{AIC}_{\Lambda\text{CDM}+\Omega_k} = -2.3. \quad (3.5)$$

The increase in preference for $q\text{CDM}+\Omega_k$ over $\Lambda\text{CDM}+\Omega_k$ comes from the fact that these datasets require a larger deviation from the cosmological constant compared to Pantheon+, as seen in the preferred values of λ (and also with the CPL parametrisation [40]). The preference for $w_0 w_a \text{CDM}+\Omega_k$ over $q\text{CDM}+\Omega_k$ is likely due to DESI + supernovae data (as seen in [40, 41]) indicating a preference for phantom-like behaviour for dark energy ($w < -1$) in the past and going towards $w > -1$ near $z \approx 0$ more rapidly than what can be obtained in the $q\text{CDM}+\Omega_k$ model.

Note however that the data does not constrain $w(z)$ directly but only indirectly through $H(z)$ and integrals of $H(z)$ that enter when calculating cosmological distances to a given redshift. In particular, $w(z)$ is well constrained close to the point $z = 0.4$ with the uncertainties increasing, especially at higher redshifts [40, 41]. Thus, to provide a good fit to the data a given quintessence model need not match the entire evolution of $w(z)$ with that in the $w_0 w_a$ model, but rather match $H(z)$ (or the distances) to a given accuracy, as pointed out in [58]. According to the latter's analysis based on this matching procedure, hilltop and plateau type models of quintessence may fit the data better as compared to the exponential model. Analysis of quintessence models from the DESI collaboration, based on parametrisations of classes of quintessence models (thawing, emergent, mirage) rather than using specific models, also finds that quintessence models can significantly improve the fit to the data w.r.t. ΛCDM [42], with the mirage class faring the best.

We also compare our results against the dark energy model-independent reconstruction of $w(z)$ using Chebyshev polynomials carried out by the DESI collaboration [41]. To do this, we plot $w(z)$ and the quantity $h(z) \equiv H(z)/H_0$ for the best-fit $q\text{CDM}+\Omega_k$ model vs the DESI reconstruction for the CMB+DESI+Union3 data combination in figure 10. We see that even though w does not go below -1, the evolution of the Hubble parameter in the best-fit $q\text{CDM}$ model matches fairly well with the DESI reconstruction. Although the deviation increases at $z \approx 0.5$, the best-fit $q\text{CDM}$ quantities still lie with the 95% confidence regions of the DESI reconstruction. It is also clear from the plots that the best-fit $q\text{CDM}$ model leads to a much lower deviation from ΛCDM compared to the reconstruction (or for that matter, the $w_0 w_a$ parametrisation).

---

[8]For flat ΛCDM we find with CMB+DESI+Union3: $\text{AIC}_{q\text{CDM}(+\Omega_k)} - \text{AIC}_{\Lambda\text{CDM}} = -1.7(-3.7)$, i.e., values similar to the $\Lambda\text{CDM}+\Omega_k$ case above (3.5).
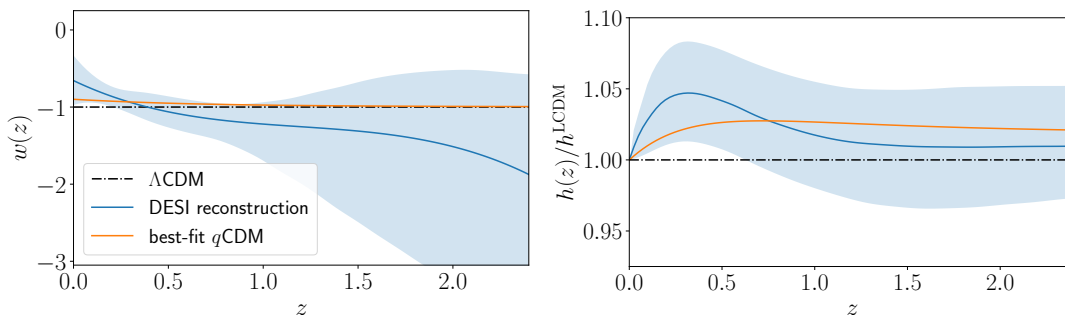
Figure 10. Evolution of $w(z)$ and $h(z) \equiv H(z)/H_0$ for the best-fit qCDM+Ω_k model compared against the DESI reconstruction using CMB+DESI+Union3 data. The shaded regions represent the 95% confidence regions for the reconstruction (data taken from figure 1 of [41]). Note that the $w_0 w_a$ evolution matches the reconstruction very well, so we do not plot it separately. At $z = 0$ we have $w_0 = -0.89$ for qCDM+Ω_k while for the reconstruction it is $w_0 = -0.65$.

4 Discussion

In this work we have performed a cosmological analysis of single field quintessence for a string theory motivated potential, namely the exponential $V = V_0 e^{-\lambda\phi}$, with open, closed or flat 3D spaces. Using the most recent cosmological data from *Planck* CMB, DESI BAO, as well as recent supernovae catalogues, we obtain the following marginalised means and limits on the potential parameter at the exponent:

$$\lambda = 0.48^{+0.28}_{-0.21}, \quad 0.68^{+0.31}_{-0.20}, \quad 0.77^{+0.18}_{-0.15}$$

at 68% C.L., by combining CMB+DESI with PantheonPlus, Union3 and DES-Y5 supernovae datasets respectively. These results indicate an increasing preference for a non-zero value of λ, where $\lambda = 0$ corresponds to a pure cosmological constant. Regarding the curvature of the 3D space slices, we find that the results point towards an open universe, $k < 0$, with the following marginalised means and limits:

$$\Omega_k = 0.0025 \pm 0.0015, \quad 0.0028^{+0.0016}_{-0.0019}, \quad 0.0027 \pm 0.0016$$

at 68% C.L., with datasets as above; the preference for non-zero curvature is, however, so far not statistically significant.

Whilst exponential quintessence is marginally favoured over ΛCDM by the cosmological data, our results indicate that the typical values for the parameter λ arising in string theory examples, conjectured to be always greater than $\sqrt{2}$ [82, 83] (see [19, 29, 33] for constructions with e.g. $\lambda = \sqrt{8/3}, \sqrt{3}$), are excluded. At the same time, given a best-fit value for λ, the dynamical system analysis that we presented (see sections 2.1 and appendix A) reveals the future evolution of the universe, in the case that dark energy is described by exponential quintessence. The observationally preferred values for λ, having $\lambda < \sqrt{2}$, indicate that — rather than having a transient phase of acceleration — the universe will evolve towards the eternally accelerating fixed point (P_ϕ or $\bar{Q}_\phi$), thus giving rise to the presence of a cosmological horizon. Alternatively, this may well indicate that the simplest single field exponential potentials are not the correct ones to describe the observed dark energy.

We have also compared our results with the CPL parametrisation used in (past and) recent cosmological studies of dynamical dark energy [40], as well as dark energy model independent reconstructions [41] of $w(z)$ using DESI and supernovae data. The data appear to prefer a more pronounced evolution of $w(z)$ than what can be obtained in the qCDM model, requiring $w(z) < -1$ in the past ($z > 1$), and rapidly growing to $w_0 > -1$ closer to the present. In contrast, for the exponential quintessence model, $w(z)$ remains very close to (but always greater than) -1 in the past, and evolves more slowly towards $w_0 > -1$ near the present. This results in a mild to moderate preference for the CPL parametrisation over our model, even though the evolution of the background quantities such as $H(z)$ in our curved exponential quintessence model is not significantly different, and still lies within the 95% confidence regions of the DESI reconstructions (see figure 10).

The hint from [41] for a phantom like equation of state for dark energy in the past is interesting from a fundamental point of view. In principle, scalar potentials arising from string theory, such as exponentials and hilltops, do all obey the energy conditions, and therefore do not give rise to phantom behaviour in a consistent way (although see [58]). However, it would be interesting to further investigate whether there can be string inspired constructions giving rise to an "effective" phantom behaviour. More generally, we emphasize the importance of developing complete fundamental scenarios that encompass the standard model as well as the dark sectors, in order to address the crucial challenges that any quintessence model presents, including time-evolution of fundamental constants, unobserved fifth forces, and the ultraviolet stability of the quintessence potential.

As we mentioned before, the present results disfavour the simplest potentials motivated by string theory constructions. On the other hand, it is fair to say that a single exponential is a rather simple case and more complex runaway exponentials could perform better, although see [84] for a no-go on string motivated potentials in supergravity. Moreover, string theory motivated hilltop potentials [85] may also perform better (see e.g. [58]). Certainly, much work is left for future studies towards systematically comparing string theory models of cosmology with current and forthcoming cosmological data.

Given that DESI will collect data over a period of five years and that the results discussed here are only based on the first year of observations, there is hope to further improve the comparison between qCDM models and the phenomenological CPL parametrisation. It would also be interesting to compare these models with other well-motivated scenarios of quintessence. At this stage it is too early to say what was (and will be!) the evolution of the dark energy equation of state parameter in our universe. Hopefully, future data from DESI as well as other dark energy focused experiments will further tighten the constraints on dark energy evolution and allow us to draw definitive conclusions on the nature of dark energy.

A Open quintessence

In this appendix we provide a short summary of the open quintessence case, which is described in detail in [29]. The cosmological equations of motion, (2.5), can be written as a dynamical system in terms of the following variables [29]:

$$x = \frac{\phi'}{\sqrt{6}}, \qquad y = \frac{\sqrt{V}}{\sqrt{3}H}, \qquad u = \frac{\sqrt{\rho_r}}{\sqrt{3}H}, \qquad z = \frac{\sqrt{-k}}{aH}, \qquad \lambda = -\frac{V_\phi}{V}, \qquad \text{(A.1)}$$

together with the constraint

$$\Omega_m = 1 - x^2 - y^2 - u^2 - z^2, \qquad \text{(A.2)}$$

where prime $'$ denotes derivative with respect to the number of efolds $\mathrm{d}N = H\mathrm{d}t$, as

$$x' = \sqrt{\frac{3}{2}} y^2 \lambda + x \left(3 \left(x^2 - 1 \right) + z^2 + \frac{3}{2}\Omega_m + 2u^2 \right), \qquad \text{(A.3a)}$$

$$y' = y \left(-\sqrt{\frac{3}{2}} x \lambda + 3 x^2 + z^2 + \frac{3}{2}\Omega_m + 2u^2 \right), \qquad \text{(A.3b)}$$

$$z' = z \left(z^2 - 1 + 3 x^2 + \frac{3}{2}\Omega_m + 2u^2 \right), \qquad \text{(A.3c)}$$

$$u' = u \left(z^2 - 2 + 3 x^2 + \frac{3}{2}\Omega_m + 2u^2 \right), \qquad \text{(A.3d)}$$

$$\lambda' = -\sqrt{6}\, x \left(\frac{\partial_\phi^2 V}{V} - \frac{(\partial_\phi V)^2}{V^2} \right), \qquad \text{(A.3e)}$$

The fixed points for this system are given in table 7 (see table 2 from [29]). The properties of the fixed points are as follows [29]:

- P_{kin} — *Kinetic domination.* The energy density is dominated by the kinetic energy of the scalar field, with $w_{\mathrm{eff}} = 1$. These points are the only fully unstable points in the past.

- P_k — *Curvature domination.* The energy density is dominated by the curvature with $\Omega_k = 1$ and $w_{\mathrm{eff}} = -1/3$. This point is a saddle.

- $P_{k\phi}$ — *Curvature scaling.* At this point, the universe evolves under the influence of both the curvature and the scalar field. However, the expansion mimics pure curvature domination with $w_{\mathrm{eff}} = -1/3$. This point exists for $\lambda > \sqrt{2}$ and it is fully stable.

- P_ϕ — *Scalar domination.* The energy density is fully dominated by the scalar field with $\Omega_\phi = 1$. This is a standard point that arises in quintessence models [30]. It exists for $\lambda < \sqrt{6}$ and is the only point that allows acceleration for $\lambda < \sqrt{2}$ with $w_{\mathrm{eff}} < -1/3$. For this value of λ, it is a stable point. It becomes a saddle for $\lambda > \sqrt{2}$.

(x,y,z,u)	Ω_m	Existence	w_{eff}
$P_{\mathrm{kin}} = (\pm 1, 0, 0, 0)$	0	$\forall\,\lambda$	1
$P_k = (0, 0, \pm 1, 0)$	0	$\forall\,\lambda$	$-\frac{1}{3}$
$P_{k\phi} = \left(\frac{1}{\lambda}\sqrt{\frac{2}{3}}, \pm\frac{2}{\lambda\sqrt{3}}, \pm\sqrt{1-\frac{2}{\lambda^2}}, 0\right)$	0	$\lambda > \sqrt{2}$ (For $\lambda = \sqrt{2}$, $P_{k\phi} = P_\phi$)	$-\frac{1}{3}$
$P_\phi = \left(\frac{\lambda}{\sqrt{6}}, \pm\frac{\sqrt{6-\lambda^2}}{\sqrt{6}}, 0, 0\right)$	0	$\lambda < \sqrt{6}$ (For $\lambda = \sqrt{6}$, $P_\phi = P_{\mathrm{kin}}$)	$\frac{\lambda^2}{3} - 1$
$P_{m\phi} = \left(\frac{1}{\lambda}\sqrt{\frac{3}{2}}, \pm\frac{1}{\lambda}\sqrt{\frac{3}{2}}, 0, 0\right)$	$1 - \frac{3}{\lambda^2}$	$\lambda > \sqrt{3}$ (For $\lambda = \sqrt{3}$, $P_{m\phi} = P_\phi$)	0
$P_m = (0, 0, 0, 0)$	1	$\forall\,\lambda$	0
$P_r = (0, 0, 0, \pm 1)$	0	$\forall\,\lambda$	$\frac{1}{3}$
$P_{r\phi} = \left(\frac{1}{\lambda}\sqrt{\frac{8}{3}}, \pm\frac{2}{\lambda\sqrt{3}}, 0, \pm\sqrt{1-\frac{4}{\lambda^2}}\right)$	0	$\lambda > 2$ (For $\lambda = 2$, $P_{r\phi} = P_\phi$)	$\frac{1}{3}$

Table 7. Fixed points for the system (A.3) (see [29]).

- $P_{m\phi}$ — *Matter scaling.* The universe evolves under the influence of both matter and scalar field. Similar to the scaling curvature point, the evolution mimics a matter dominated epoch with $w_{\mathrm{eff}} = 0$. This point is a saddle.

- P_m — *Matter domination.* The energy density is dominated by matter with $\Omega_m = 1$ and $w_{\mathrm{eff}} = 0$ and it is a saddle.

- P_r — *Radiation domination.* The energy density is dominated by radiation with $\Omega_r = 1$ and $w_{\mathrm{eff}} = \frac{1}{3}$. This point is also a saddle.

- $P_{r\phi}$ — *Radiation scaling.* The universe evolves under influence of radiation and the scalar field. As the other scaling points, it mimics a pure radiation domination universe with $w_{\mathrm{eff}} = \frac{1}{3}$.

The stability of the fixed points in the open quintessence can be found in table 3 of [29], which we reproduce in our table 8.

Point	Eigenvalues	Stability	Existence
$P_{\text{kin}}^{\pm}$	$\left(3, 2, 3 \mp \lambda\sqrt{\frac{3}{2}}, 1\right)$	P_{kin}^{+}: Fully unstable P_{kin}^{-}: Fully unstable for $\lambda \leq \sqrt{6}$ P_{kin}^{-}: Saddle for $\lambda > \sqrt{6}$	—
P_k	$(-2, -1, 1, -1)$	Saddle	—
$P_{k\phi}$	$\left(-1, -1 - \frac{\sqrt{8-3\lambda^2}}{\lambda}, -1 + \frac{\sqrt{8-3\lambda^2}}{\lambda}, -1\right)$	Stable	$\lambda > \sqrt{2}$
P_ϕ	$\left(\frac{\lambda^2}{2} - 3, \lambda^2 - 3, \frac{\lambda^2}{2} - 1, \frac{\lambda^2}{2} - 2\right)$	Stable for $\lambda < \sqrt{2}$ Saddle for $\lambda > \sqrt{2}$	$\lambda < \sqrt{6}$
$P_{m\phi}$	$\left(\frac{1}{2}, -\frac{3(\lambda+\sqrt{24-7\lambda^2})}{4\lambda}, -\frac{3(\lambda-\sqrt{24-7\lambda^2})}{4\lambda}, -\frac{1}{2}\right)$	Saddle	$\lambda > \sqrt{3}$
P_m	$(-\frac{3}{2}, \frac{3}{2}, \frac{1}{2}, -\frac{1}{2})$	Saddle	—
P_r	$(-1, 2, 1, 1)$	Saddle	—
$P_{r\phi}$	$(1, 1, -\frac{\lambda+\sqrt{64-15\lambda^2}}{2\lambda}, -\frac{\lambda-\sqrt{64-15\lambda^2}}{2\lambda})$	Saddle	$\lambda > 2$

Table 8. Stability of the fixed points in table 7 (see reference [29] for details).

B   Full cosmological constraints

In this appendix we collect the results for the constraints on the full set of cosmological parameters in figure 11 and table 9 for the CMB+DESI data as well as with the addition of the various supernovae data described before. In figure 12 and table 10 we compare the constraints on the parameters using CMB+DESI+Pantheon+ vs CMB+SDSS+Pantheon+. Finally, in figure 13 we show the constraints for the exponential quintessence model under the assumption of flat spatial geometry of the universe.
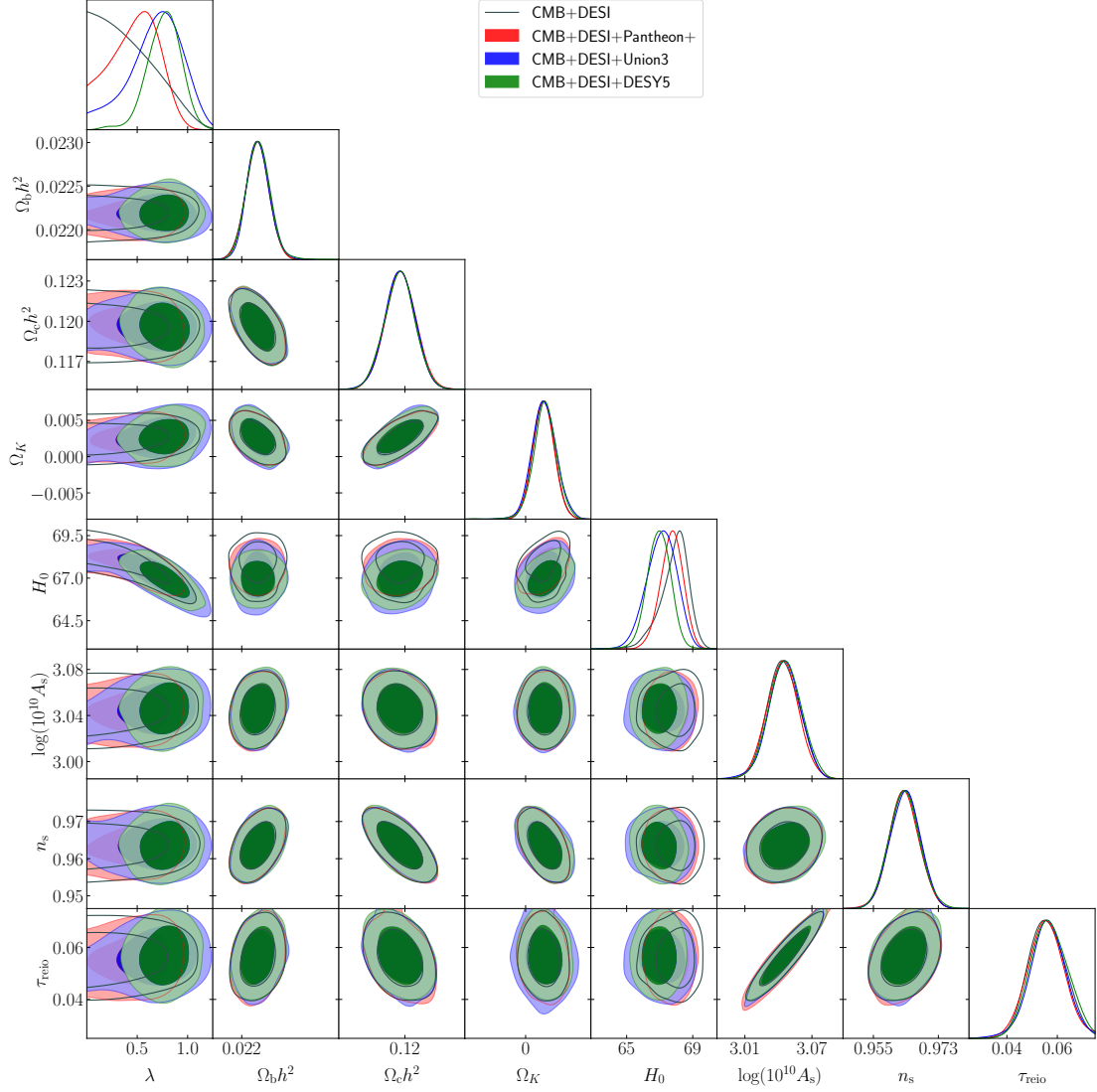
Figure 11. Constraints on the full set of cosmological parameters for CMB+DESI as well as with the addition of the different supernovae datasets.

Parameter	CMB+DESI	+Pantheon+	+Union3+	+DESY5
λ	< 0.537	$0.48^{+0.28}_{-0.21}$	$0.68^{+0.31}_{-0.20}$	$0.77^{+0.18}_{-0.15}$
Ω_k	0.0026 ± 0.0015	0.0025 ± 0.0015	$0.0028^{+0.0016}_{-0.0019}$	0.0027 ± 0.0016
$\Omega_c h^2$	0.1196 ± 0.0012	0.1197 ± 0.0012	0.1195 ± 0.0012	0.1195 ± 0.0012
$\log(10^{10} A_s)$	3.045 ± 0.014	3.044 ± 0.014	3.049 ± 0.013	3.047 ± 0.014
n_s	0.9636 ± 0.0041	0.9635 ± 0.0041	0.9640 ± 0.0041	0.9637 ± 0.0047
H_0	$67.89^{+0.96}_{-0.61}$	$67.73^{+0.72}_{-0.64}$	$67.12^{+0.97}_{-0.83}$	66.95 ± 0.72
$\Omega_b h^2$	0.02219 ± 0.00014	0.02219 ± 0.00013	$0.02220^{+0.00013}_{-0.00015}$	0.02221 ± 0.00013
τ_{reio}	0.0559 ± 0.0071	0.0554 ± 0.0072	0.0571 ± 0.0067	0.0577 ± 0.0069

Table 9. Parameter means and 68% limits.

Parameter	CMB+DESI+Pantheon+	CMB+SDSS+Pantheon+
λ	$0.48^{+0.28}_{-0.21}$	$0.40^{+0.20}_{-0.29}$
Ω_k	0.0025 ± 0.0015	0.0014 ± 0.0017
$\Omega_c h^2$	0.1197 ± 0.0012	$0.1197^{+0.0013}_{-0.0012}$
$\log(10^{10} A_s)$	3.044 ± 0.014	3.046 ± 0.014
n_s	0.9635 ± 0.0041	0.9639 ± 0.0043
H_0	$67.73^{+0.72}_{-0.64}$	67.44 ± 0.64
$\Omega_b h^2$	0.02219 ± 0.00013	$0.02220^{+0.00013}_{-0.00016}$
τ_{reio}	0.0554 ± 0.0072	0.0562 ± 0.0065

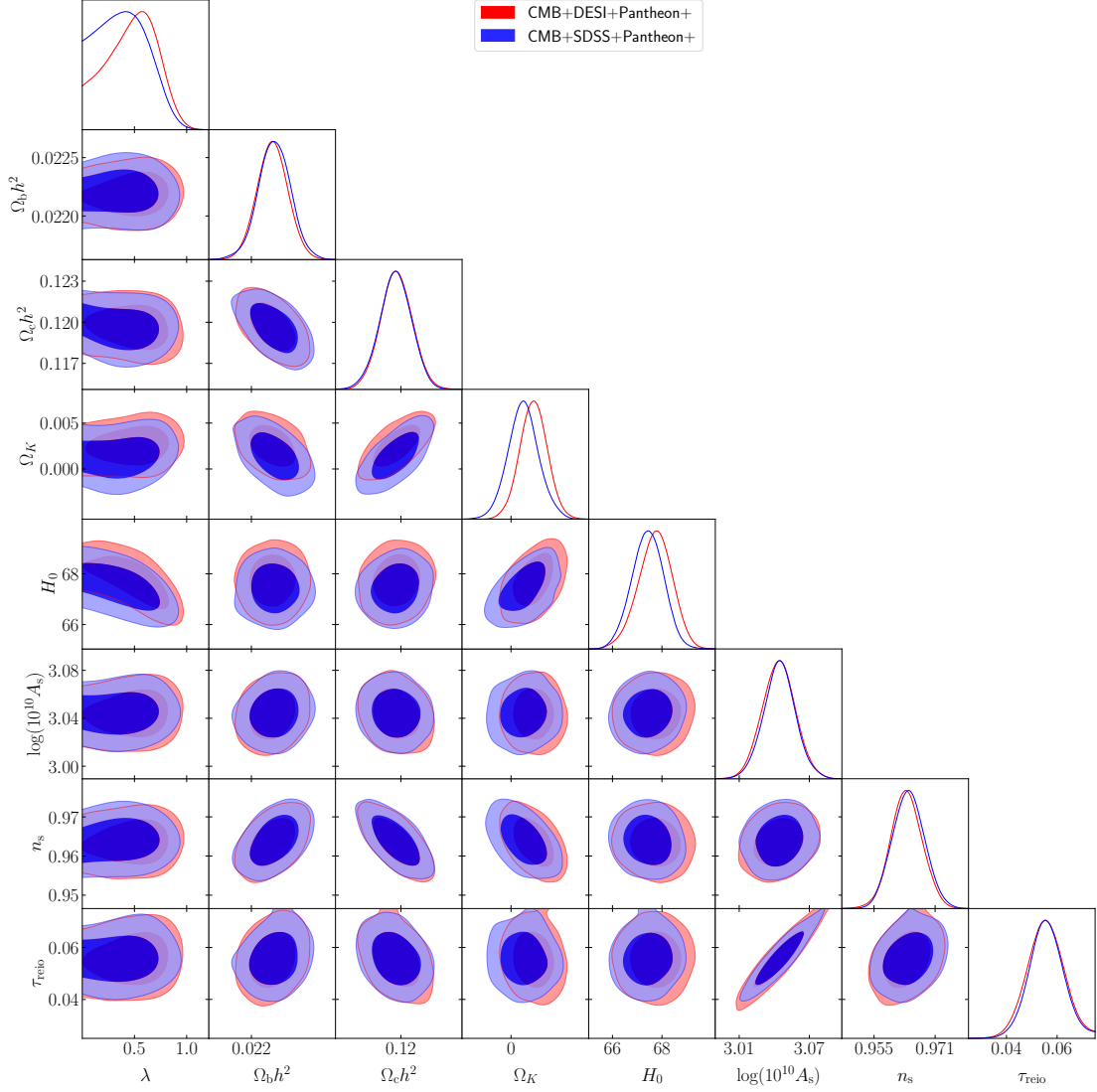**Table 10.** Parameter means and 68% limits.

Figure 12. Constraints on cosmological parameters for CMB+DESI+Pantheon+ and CMB+SDSS+Pantheon+.
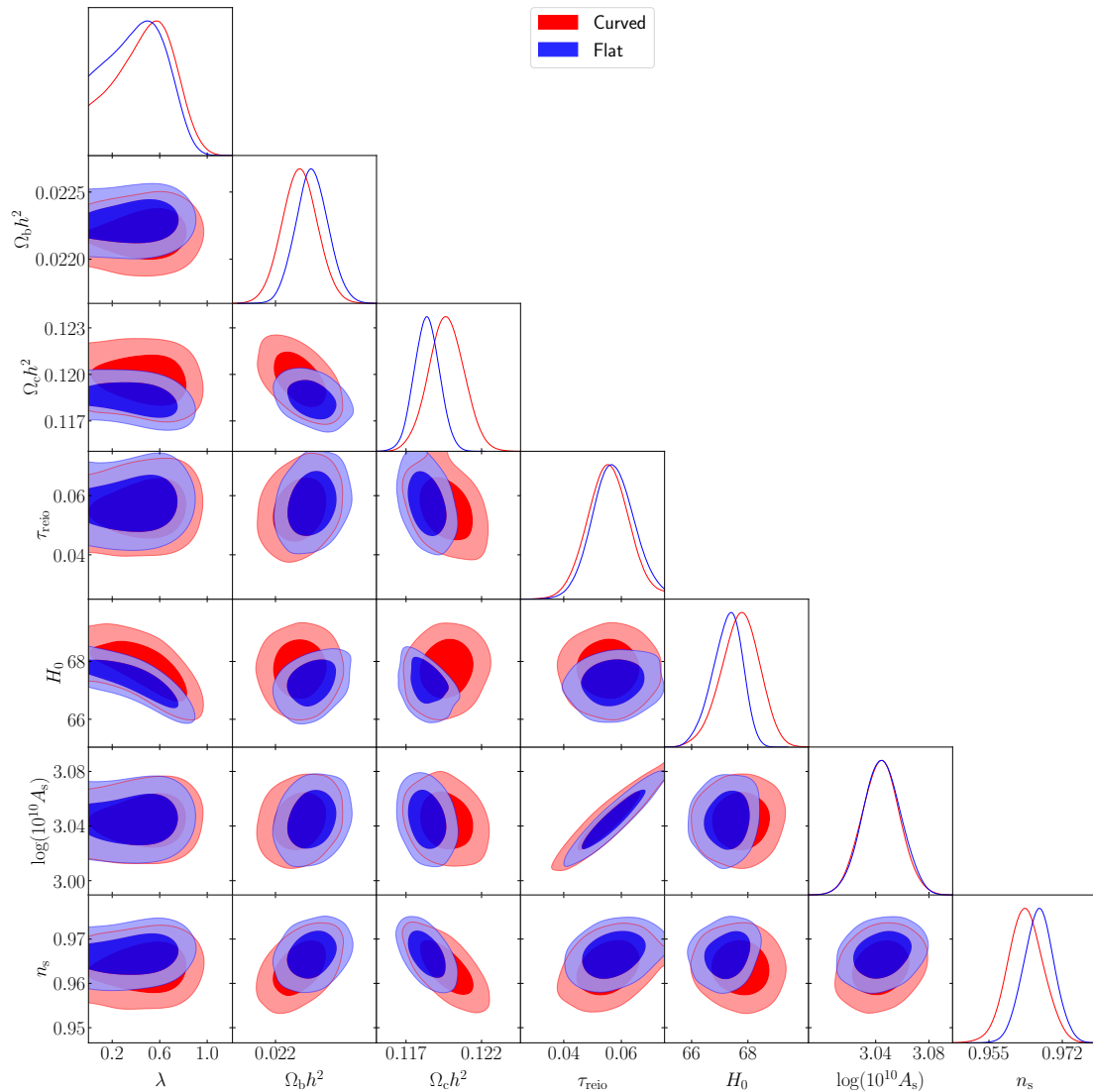
Figure 13. Comparison of the exponential quintessence model analysed in the main text with curved vs flat spatial geometry for CMB+DESI+Pantheon+. The constraints are slightly relaxed for the model with non-zero Ω_k but there is no major shift in any cosmological parameter. In particular, the marginalised distribution of λ does not show a significant difference. Note that for the curved case, the constraints shown are obtained after marginalising over Ω_k.

References

[1] SUPERNOVA SEARCH TEAM collaboration, *Observational evidence from supernovae for an accelerating universe and a cosmological constant*, *Astron. J.* **116** (1998) 1009 [astro-ph/9805201] [INSPIRE].

[2] SUPERNOVA COSMOLOGY PROJECT collaboration, *Measurements of Ω and Λ from 42 High Redshift Supernovae*, *Astrophys. J.* **517** (1999) 565 [astro-ph/9812133] [INSPIRE].

[3] E. Abdalla et al., *Cosmology intertwined: A review of the particle physics, astrophysics, and cosmology associated with the cosmological tensions and anomalies*, *JHEAp* **34** (2022) 49 [arXiv:2203.06142] [INSPIRE].

[4] W. Fischler, A. Kashani-Poor, R. McNees and S. Paban, *The acceleration of the universe, a challenge for string theory*, *JHEP* **07** (2001) 003 [hep-th/0104181] [INSPIRE].

[5] S. Hellerman, N. Kaloper and L. Susskind, *String theory and quintessence*, *JHEP* **06** (2001) 003 [hep-th/0104180] [INSPIRE].

[6] M. Cicoli et al., *String cosmology: From the early universe to today*, *Phys. Rept.* **1059** (2024) 1 [arXiv:2303.04819] [INSPIRE].

[7] S.K. Garg and C. Krishnan, *Bounds on Slow Roll and the de Sitter Swampland*, *JHEP* **11** (2019) 075 [arXiv:1807.05193] [INSPIRE].

[8] H. Ooguri, E. Palti, G. Shiu and C. Vafa, *Distance and de Sitter Conjectures on the Swampland*, *Phys. Lett. B* **788** (2019) 180 [arXiv:1810.05506] [INSPIRE].

[9] B. Ratra and P.J.E. Peebles, *Cosmological Consequences of a Rolling Homogeneous Scalar Field*, *Phys. Rev. D* **37** (1988) 3406 [INSPIRE].

[10] P.J.E. Peebles and B. Ratra, *Cosmology with a Time Variable Cosmological Constant*, *Astrophys. J. Lett.* **325** (1988) L17 [INSPIRE].

[11] R.R. Caldwell, R. Dave and P.J. Steinhardt, *Cosmological imprint of an energy component with general equation of state*, *Phys. Rev. Lett.* **80** (1998) 1582 [astro-ph/9708069] [INSPIRE].

[12] E.J. Copeland, A.R. Liddle and D. Wands, *Exponential potentials and cosmological scaling solutions*, *Phys. Rev. D* **57** (1998) 4686 [gr-qc/9711068] [INSPIRE].

[13] J.M. Cline, *Quintessence, cosmological horizons, and self-tuning*, *JHEP* **08** (2001) 035 [hep-ph/0105251] [INSPIRE].

[14] C.F. Kolda and W. Lahneman, *Exponential quintessence and the end of acceleration*, hep-ph/0105300 [INSPIRE].

[15] P. Agrawal, G. Obied, P.J. Steinhardt and C. Vafa, *On the Cosmological Implications of the String Swampland*, *Phys. Lett. B* **784** (2018) 271 [arXiv:1806.09718] [INSPIRE].

[16] Y. Akrami, R. Kallosh, A. Linde and V. Vardanyan, *The Landscape, the Swampland and the Era of Precision Cosmology*, *Fortsch. Phys.* **67** (2019) 1800075 [arXiv:1808.09440] [INSPIRE].

[17] M. Raveri, W. Hu and S. Sethi, *Swampland Conjectures and Late-Time Cosmology*, *Phys. Rev. D* **99** (2019) 083518 [arXiv:1812.10448] [INSPIRE].

[18] N. Schöneberg et al., *News from the Swampland — constraining string theory with astrophysics and cosmology*, *JCAP* **10** (2023) 039 [arXiv:2307.15060] [INSPIRE].

[19] D. Andriot, D. Tsimpis and T. Wrase, *Accelerated expansion of an open universe and string theory realizations*, *Phys. Rev. D* **108** (2023) 123515 [arXiv:2309.03938] [INSPIRE].

[20] L.J. Boya, M.A. Per and A.J. Segui, *Graphical and kinematical approach to cosmological horizons*, *Phys. Rev. D* **66** (2002) 064009 [gr-qc/0203074] [INSPIRE].

[21] B. Freivogel, M. Kleban, M. Rodriguez Martinez and L. Susskind, *Observational consequences of a landscape*, *JHEP* **03** (2006) 039 [hep-th/0505232] [INSPIRE].

[22] S. Cespedes, S.P. de Alwis, F. Muia and F. Quevedo, *Lorentzian vacuum transitions: Open or closed universes?*, *Phys. Rev. D* **104** (2021) 026013 [arXiv:2011.13936] [INSPIRE].

[23] S. Cespedes, S. de Alwis, F. Muia and F. Quevedo, *Quantum transitions, detailed balance, black holes, and nothingness*, *Phys. Rev. D* **109** (2024) 105027 [arXiv:2307.13614] [INSPIRE].

[24] R. Bousso and E. Wildenhain, *Islands in closed and open universes*, *Phys. Rev. D* **105** (2022) 086012 [arXiv:2202.05278] [INSPIRE].

[25] I. Ben-Dayan, M. Hadad and E. Wildenhain, *Islands in the fluid: islands are common in cosmology*, *JHEP* **03** (2023) 077 [arXiv:2211.16600] [INSPIRE].

[26] A. Almheiri et al., *The entropy of Hawking radiation*, *Rev. Mod. Phys.* **93** (2021) 035002 [arXiv:2006.06872] [INSPIRE].

[27] N. Engelhardt and A.C. Wall, *Quantum Extremal Surfaces: Holographic Entanglement Entropy beyond the Classical Regime*, *JHEP* **01** (2015) 073 [arXiv:1408.3203] [INSPIRE].

[28] T. Hartman, Y. Jiang and E. Shaghoulian, *Islands in cosmology*, *JHEP* **11** (2020) 111 [arXiv:2008.01022] [INSPIRE].

[29] D. Andriot et al., *Exponential quintessence: curved, steep and stringy?*, *JHEP* **08** (2024) 117 [arXiv:2405.09323] [INSPIRE].

[30] S. Bahamonde et al., *Dynamical systems applied to cosmology: dark energy and modified gravity*, *Phys. Rept.* **775-777** (2018) 1 [arXiv:1712.03107] [INSPIRE].

[31] R.J. van den Hoogen, A.A. Coley and D. Wands, *Scaling solutions in Robertson-Walker space-times*, *Class. Quant. Grav.* **16** (1999) 1843 [gr-qc/9901014] [INSPIRE].

[32] M. Gosenca and P. Coles, *Dynamical Analysis of Scalar Field Cosmologies with Spatial Curvature*, *Open J. Astrophys.* **1** (2016) 1 [arXiv:1502.04020] [INSPIRE].

[33] P. Marconnet and D. Tsimpis, *Universal accelerating cosmologies from 10d supergravity*, *JHEP* **01** (2023) 033 [arXiv:2210.10813] [INSPIRE].

[34] A. Savaş Arapoğlu and A. Emrah Yükselci, *Dynamical System Analysis of Quintessence Models with Exponential Potential — Revisited*, *Mod. Phys. Lett. A* **34** (2019) 1950069 [arXiv:1711.03824] [INSPIRE].

[35] DES collaboration, *The Dark Energy Survey: Cosmology Results With ∼1500 New High-redshift Type Ia Supernovae Using The Full 5-year Dataset*, arXiv:2401.02929 [INSPIRE].

[36] DESI collaboration, *DESI 2024 IV: Baryon Acoustic Oscillations from the Lyman Alpha Forest*, arXiv:2404.03001 [INSPIRE].

[37] EUCLID collaboration, *Euclid preparation. VII. Forecast validation for Euclid cosmological probes*, *Astron. Astrophys.* **642** (2020) A191 [arXiv:1910.09273] [INSPIRE].

[38] LSST SCIENCE and LSST PROJECT collaborations, *LSST Science Book, Version 2.0*, arXiv:0912.0201 [INSPIRE].

[39] DESI collaboration, *DESI 2024 III: Baryon Acoustic Oscillations from Galaxies and Quasars*, arXiv:2404.03000 [INSPIRE].

[40] DESI collaboration, *DESI 2024 VI: Cosmological Constraints from the Measurements of Baryon Acoustic Oscillations*, arXiv:2404.03002 [INSPIRE].

[41] DESI collaboration, *DESI 2024: Reconstructing Dark Energy using Crossing Statistics with DESI DR1 BAO data*, arXiv:2405.04216 [INSPIRE].

[42] DESI collaboration, *DESI 2024: Constraints on Physics-Focused Aspects of Dark Energy using DESI DR1 BAO Data*, arXiv:2405.13588 [INSPIRE].

[43] E.Ó. Colgáin et al., *Does DESI 2024 Confirm ΛCDM?*, arXiv:2404.08633 [INSPIRE].

[44] Y. Carloni, O. Luongo and M. Muccino, *Does dark energy really revive using DESI 2024 data?*, arXiv:2404.12068 [INSPIRE].

[45] C.-G. Park, J. de Cruz Perez and B. Ratra, *Using non-DESI data to confirm and strengthen the DESI 2024 spatially-flat w_0w_aCDM cosmological parameterization result*, arXiv:2405.00502 [INSPIRE].

[46] D. Wang, *The Self-Consistency of DESI Analysis and Comment on "Does DESI 2024 Confirm ΛCDM?"*, arXiv:2404.13833 [INSPIRE].

[47] M. Cortês and A.R. Liddle, *Interpreting DESI's evidence for evolving dark energy*, arXiv:2404.08056 [INSPIRE].

[48] Z. Wang, S. Lin, Z. Ding and B. Hu, *The role of LRG1 and LRG2's monopole in inferring the DESI 2024 BAO cosmology*, arXiv:2405.02168 [INSPIRE].

[49] B.R. Dinda, *A new diagnostic for the null test of dynamical dark energy in light of DESI 2024 and other BAO data*, arXiv:2405.06618 [INSPIRE].

[50] K.S. Croker et al., *DESI Dark Energy Time Evolution is Recovered by Cosmologically Coupled Black Holes*, arXiv:2405.12282 [INSPIRE].

[51] D. Wang, *Constraining Cosmological Physics with DESI BAO Observations*, arXiv:2404.06796 [INSPIRE].

[52] O. Luongo and M. Muccino, *Model independent cosmographic constraints from DESI 2024*, arXiv:2404.07070 [INSPIRE].

[53] P. Mukherjee and A.A. Sen, *Model-independent cosmological inference post DESI DR1 BAO measurements*, arXiv:2405.19178 [INSPIRE].

[54] H. Wang and Y.-S. Piao, *Dark energy in light of recent DESI BAO and Hubble tension*, arXiv:2404.18579 [INSPIRE].

[55] Y. Tada and T. Terada, *Quintessential interpretation of the evolving dark energy in light of DESI observations*, *Phys. Rev. D* **109** (2024) L121305 [arXiv:2404.05722] [INSPIRE].

[56] W. Yin, *Cosmic clues: DESI, dark energy, and the cosmological constant problem*, *JHEP* **05** (2024) 327 [arXiv:2404.06444] [INSPIRE].

[57] K.V. Berghaus, J.A. Kable and V. Miranda, *Quantifying Scalar Field Dynamics with DESI 2024 Y1 BAO measurements*, arXiv:2404.14341 [INSPIRE].

[58] D. Shlivko and P.J. Steinhardt, *Assessing observational constraints on dark energy*, *Phys. Lett. B* **855** (2024) 138826 [arXiv:2405.03933] [INSPIRE].

[59] M. Chevallier and D. Polarski, *Accelerating universes with scaling dark matter*, *Int. J. Mod. Phys. D* **10** (2001) 213 [gr-qc/0009008] [INSPIRE].

[60] E.V. Linder, *Exploring the expansion history of the universe*, *Phys. Rev. Lett.* **90** (2003) 091301 [astro-ph/0208512] [INSPIRE].

[61] R. Aurich and F. Steiner, *Quintessence and the curvature of the universe after wmap*, *Int. J. Mod. Phys. D* **13** (2004) 123 [astro-ph/0302264] [INSPIRE].

[62] D. Brout et al., *The Pantheon+ Analysis: Cosmological Constraints*, *Astrophys. J.* **938** (2022) 110 [arXiv:2202.04077] [INSPIRE].

[63] D. Rubin et al., *Union Through UNITY: Cosmology with 2,000 SNe Using a Unified Bayesian Framework*, arXiv:2311.12098 [INSPIRE].

[64] G. Alestas et al., *To curve, or not to curve: Is curvature-assisted quintessence observationally viable?*, arXiv:2406.09212 [INSPIRE].

[65] O.F. Ramadan, J. Sakstein and D. Rubin, *DESI constraints on exponential quintessence*, *Phys. Rev. D* **110** (2024) L041303 [arXiv:2405.18747] [INSPIRE].

[66] A. Lewis, A. Challinor and A. Lasenby, *Efficient computation of CMB anisotropies in closed FRW models*, *Astrophys. J.* **538** (2000) 473 [astro-ph/9911177] [INSPIRE].

[67] C. Howlett, A. Lewis, A. Hall and A. Challinor, *CMB power spectrum parameter degeneracies in the era of precision cosmology*, *JCAP* **04** (2012) 027 [arXiv:1201.3654] [INSPIRE].

[68] PLANCK collaboration, *Planck 2018 results. V. CMB power spectra and likelihoods*, *Astron. Astrophys.* **641** (2020) A5 [arXiv:1907.12875] [INSPIRE].

[69] E. Rosenberg, S. Gratton and G. Efstathiou, *CMB power spectra and cosmological parameters from Planck PR4 with CamSpec*, *Mon. Not. Roy. Astron. Soc.* **517** (2022) 4620 [arXiv:2205.10869] [INSPIRE].

[70] PLANCK collaboration, *Planck 2018 results. VIII. Gravitational lensing*, *Astron. Astrophys.* **641** (2020) A8 [arXiv:1807.06210] [INSPIRE].

[71] eBOSS collaboration, *Completed SDSS-IV extended Baryon Oscillation Spectroscopic Survey: Cosmological implications from two decades of spectroscopic surveys at the Apache Point Observatory*, *Phys. Rev. D* **103** (2021) 083533 [arXiv:2007.08991] [INSPIRE].

[72] A. Lewis and S. Bridle, *Cosmological parameters from CMB and other data: A Monte Carlo approach*, *Phys. Rev. D* **66** (2002) 103511 [astro-ph/0205436] [INSPIRE].

[73] A. Lewis, *Efficient sampling of fast and slow cosmological parameters*, *Phys. Rev. D* **87** (2013) 103529 [arXiv:1304.4473] [INSPIRE].

[74] J. Torrado and A. Lewis, *Cobaya: Code for Bayesian Analysis of hierarchical physical models*, *JCAP* **05** (2021) 057 [arXiv:2005.05290] [INSPIRE].

[75] A. Lewis, *GetDist: a Python package for analysing Monte Carlo samples*, arXiv:1910.13970 [INSPIRE].

[76] C. Cartis, L. Roberts and O. Sheridan-Methven, *Escaping local minima with local derivative-free methods: a numerical investigation*, *Optimization* **71** (2021) 2343 [arXiv:1812.11343] [INSPIRE].

[77] C. Cartis, J. Fiala, B. Marteau and L. Roberts, *Improving the Flexibility and Robustness of Model-Based Derivative-Free Optimization Solvers*, arXiv:1804.00154 [INSPIRE].

[78] E.Ó. Colgáin and H. Yavartanoo, *Testing the Swampland: H_0 tension*, *Phys. Lett. B* **797** (2019) 134907 [arXiv:1905.02555] [INSPIRE].

[79] A. Banerjee et al., *Hubble sinks in the low-redshift swampland*, *Phys. Rev. D* **103** (2021) L081305 [arXiv:2006.00244] [INSPIRE].

[80] A.R. Liddle, *How many cosmological parameters?*, *Mon. Not. Roy. Astron. Soc.* **351** (2004) L49 [astro-ph/0401198] [INSPIRE].

[81] H. Akaike, *A new look at the statistical model identification*, *IEEE Trans. Automatic Control* **19** (1974) 716 [InSPIRE].

[82] A. Bedroya and C. Vafa, *Trans-Planckian Censorship and the Swampland*, *JHEP* **09** (2020) 123 [arXiv:1909.11063] [InSPIRE].

[83] T. Rudelius, *Dimensional reduction and (Anti) de Sitter bounds*, *JHEP* **08** (2021) 041 [arXiv:2101.11617] [InSPIRE].

[84] B. Valeixo Bento, D. Chakraborty, S.L. Parameswaran and I. Zavala, *Dark Energy in String Theory*, *PoS* **CORFU2019** (2020) 123 [arXiv:2005.10168] [InSPIRE].

[85] Y. Olguin-Trejo, S.L. Parameswaran, G. Tasinato and I. Zavala, *Runaway Quintessence, Out of the Swampland*, *JCAP* **01** (2019) 031 [arXiv:1810.08634] [InSPIRE].